Research Square

Preprints are preliminary reports that have not undergone peer review.
They should not be considered conclusive, used to inform clinical practice,
or referenced by the media as validated information.

Strain-Rate Dependence of Mode II Delamination Initiation in a Polyester-Fiberglass Composite Using Dynamic ENF Testing

Ali Javed

ali_javed18@yahoo.com

Institute of Space Technology

Owais Shah

Institute of Space Technology

Research Article

Keywords: Strain Energy Release Rate, End Notched Flexural tests, 3 point bending, Split Hopkinson Pressure Bar

Posted Date: November 2nd, 2026

DOI: https://doi.org/10.21203/rs.3.rs-11305278/v1

License: This work is licensed under a Creative Commons Attribution 4.0 International License.
Read Full License

Additional Declarations: No competing interests reported.

Strain-Rate Dependence of Mode II Delamination Initiation in a Polyester-Fiberglass Composite Using Dynamic ENF Testing

[1]Ali Javed*, [1]Dr Owais ur Rehman Shah

ali_javed18@yahoo.com, owaisurrehmanshah41@gmail.com

[1]Institute of Space Technology, Islamabad, Pakistan

*Corresponding Author: ali_javed18@yahoo.com

ABSTRACT

The inter-laminar crack growth resistance in fiber-reinforced composites under Mode II (shear) loading is a critical factor for structural integrity in dynamic environments. Traditional End Notched Flexural (ENF) tests have been extensively used under static conditions, yet limited studies exist on high strain rate effects using dynamic setups.

The objective of this study is to investigate the influence of varying strain rates on the Mode II strain energy release rate G_{IIi} at damage initiation for polyester-fiberglass composites using a dynamic loading approach. ENF specimens composed of ±45° glass fiber mats and polyester resin were subjected to three-point bending under different strain rates ranging from 70 s^{-1} to 150 s^{-1} using a Split Hopkinson Pressure Bar (SHPB) system. High-speed imaging was employed to capture damage progression, and Mode II SERR was computed using beam theory formulations based on force and displacement data. The results demonstrate a clear trend of increasing G_{IIi} with elevated strain rates, rising from 0.64 to 7.19 kJ/m². The average increase in dynamic crack propagation energy was observed to exceed values from static testing. However, observed failure modes included fiber bridging and non-planar crack paths, contributing to variability in measured results. The dynamic ENF testing shows that Mode II fracture energy in polyester-fiberglass composites is strongly strain rate dependent. The results suggest the need for longer specimen geometries to ensure stable inter-laminar propagation in future investigations.

Keywords— Strain Energy Release Rate, End Notched Flexural tests, 3 point bending, Split Hopkinson Pressure Bar.

1. INTRODUCTION

The inter-laminar crack growth resistance in plane shearing is classically measured using the End Notched Flexural or ENF [1] tests. Crack growth resistance is one of the fundamental design parameters that must be characterized for any composite structure. Inter-laminar (delamination) crack propagation is the most common case of interest, and it is typically studied by introducing an artificial pre-crack at one of the ply interfaces and loading the specimen to generate either shear or normal stresses at the crack tip. In the present study, plane shear loading is used to drive crack propagation in what is commonly referred to in the fracture mechanics literature as Mode II.

The determination of these crack propagation energies has been treated under dynamic loadings [2], [3] and has shown a relation of dissipated strain energy to the loading rate.

The specimens are loaded under 3 point bending loads, to create plane shear at the crack interface. The specimens are loaded in bending using a special mounting fixed to compression type split Hopkinson pressure bars [4], [5], which are used for characterizing the damage characteristics of composite materials [6], [7]. The experimental procedure shall be discussed in the corresponding sections.

Beyond the fundamental principle of the SHPB itself, first established by Hopkinson [30] and later refined by Kolsky [31] for measuring dynamic mechanical response at high strain rates, several studies have applied modified Hopkinson bar configurations specifically to fracture initiation problems, including three-point bending fracture toughness measurements [32] and semi-circular bend geometries [33].

Within composite materials specifically, the rate-dependence of Mode II interlaminar toughness has received growing attention over the past decade. Zabala et al. [11] developed a dynamic four-point ENF (4ENF) procedure for unidirectional carbon/epoxy composites to obtain full dynamic R-curves, while Yasaee et al. [12] used a modified Hopkinson bar together with drop-weight and servo-hydraulic rigs to span quasi-static to 5 m/s loading rates on Z-pinned and unreinforced laminates. Shamchi et al. [13] applied a similar dynamic three-point bending approach, based on the split Hopkinson bar principle, to electrically modified carbon/epoxy ENF specimens up to 5.5 m/s. Machado et al. [14] specifically examined the combined influence of loading rate (0.2 and 11 s^{-1}) and temperature on GIIC of CFRP ENF specimens, while Low et al. [15] reported that GIIC

of carbon/epoxy ENF specimens increased by up to 45% with displacement rate, attributing the increase to a transition from interfacial debonding to matrix-dominated shear-cusp failure. May et al. [16] reviewed the state of high-rate Mode II fracture toughness testing methods more broadly and highlighted the continued lack of a standardized approach at high loading rates — a gap the present study's SHPB-based ENF method aims to help address.

Historically, the earliest systematic investigations of rate effects on interlaminar fracture toughness were carried out on graphite/epoxy systems using DCB and ENF configurations. Smiley and Pipes [17] showed that Mode I toughness of graphite/epoxy and graphite/PEEK laminates decreased with increasing opening rate, while Aliyu and Daniel [18] and Daniel et al. [19] extended this to both untoughened and toughened graphite/epoxy systems, and Daniel et al. [25] characterized strain-rate effects on unidirectional graphite/epoxy more generally. Russell and Street [23] additionally considered moisture and temperature interactions with mixed-mode delamination rate sensitivity. Friedrich et al. [24] proposed underlying micromechanical explanations for these rate effects, relating fracture-surface morphology changes to the observed toughness trends, a theme echoed in the fractographic studies of Gilchrist and Svensson [27], Boll et al. [40], and the matrix-cracking analysis of Liu et al. [39] and Wang et al. [38].

Since the present specimens are a glass-fiber/polyester system rather than carbon/epoxy, the closely related work of de Morais et al. [20] on Mode II ENF testing of filament-wound glass/polyester angle-ply laminates, and of Ekeoseye et al. [21] on flax/glass/epoxy hybrid ENF specimens, is particularly relevant, as both report the non-planar crack paths and fiber-bridging effects also observed in the present study. Carlsson et al. [22] similarly reported Mode II interlaminar fracture behavior for glass/epoxy and PEEK-based systems using early ENF specimen designs.

Correct interpretation of ENF load–displacement data also depends on proper specimen sizing and beam-theory corrections. Ozdil et al. [26] derived beam analysis corrections for angle-ply ENF laminates, and Davidson et al. [27] provided three-dimensional design recommendations for both unidirectional and multidirectional ENF geometries — considerations directly relevant to the a_0/L ratio and specimen geometry adopted here. Finally, at the material-response level, Jacob et al. [28] and Gerlach et al. [29] demonstrated pronounced strain-rate sensitivity of fracture toughness and stiffness in random-chopped-fiber and GFRP systems respectively, reinforcing the expectation that

polyester-fiberglass composites of the type used in this study should likewise exhibit measurable rate dependence.

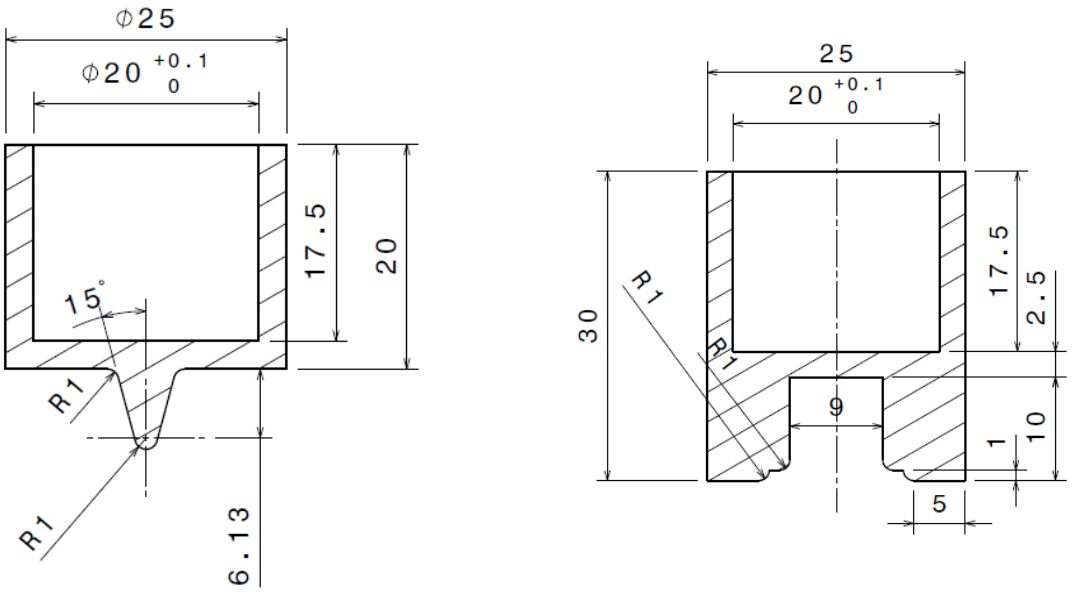
2. METHODOLOGY

A. Experimental Setup

The specimens are made up of polyester resin reinforced with glass fibers. The glass fiber mat used is a ±45° biax mat, plied in 7 layers to make up the desired 4mm thickness. The specimens are 13 x 13mm with a pre-crack at 4.55mm long. The pre-crack has been chosen as such to have a pre-crack to span or a_o/L ratio of 0.35, which has been found out to be the ratio for stable crack growth for such materials, under precedent static crack propagation tests [8].

The Split Pressure Hopkinson Bar used for these experiments has a maximum loading ability of up to 2000 s^{-1} strain rates. However, for our experiments we shall be limited to a value much lower than this limit.

The supports shown in the figure 1 are fixed at the bar ends to apply a 3 point bending load on the ENF specimens. Furthermore, a high speed camera filming at 100000 images per second is used to film the failure phenomena taking place during these tests.



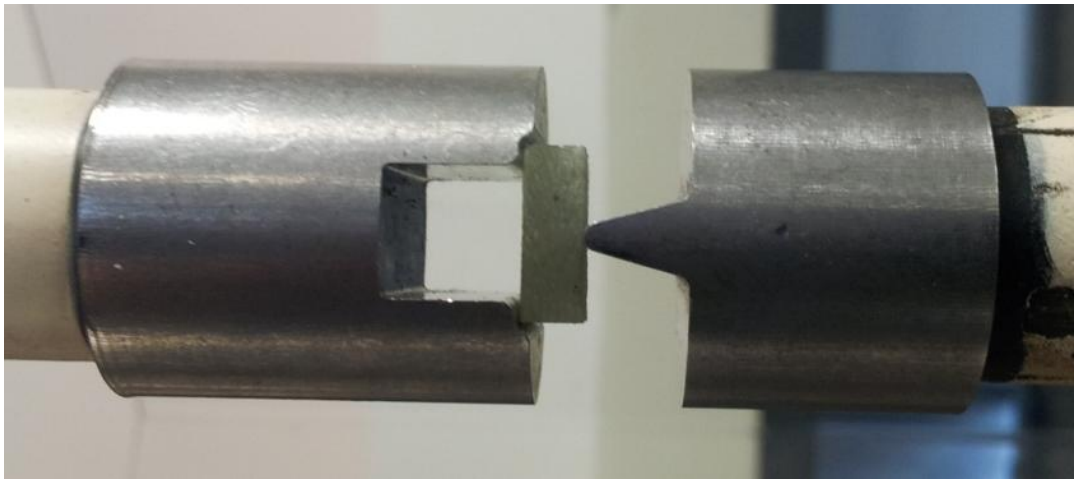


Figure 1: Fixation used to apply 3 point bending load using the SHPB apparatus.

a. Principle of the SHPB

The Split Hopkinson Pressure Bar or SHPB in short also called the Split Kolsky Pressure Bar or SKPB is an apparatus which is used for the identification of material properties at different applied strain rates as shown in figure 2.

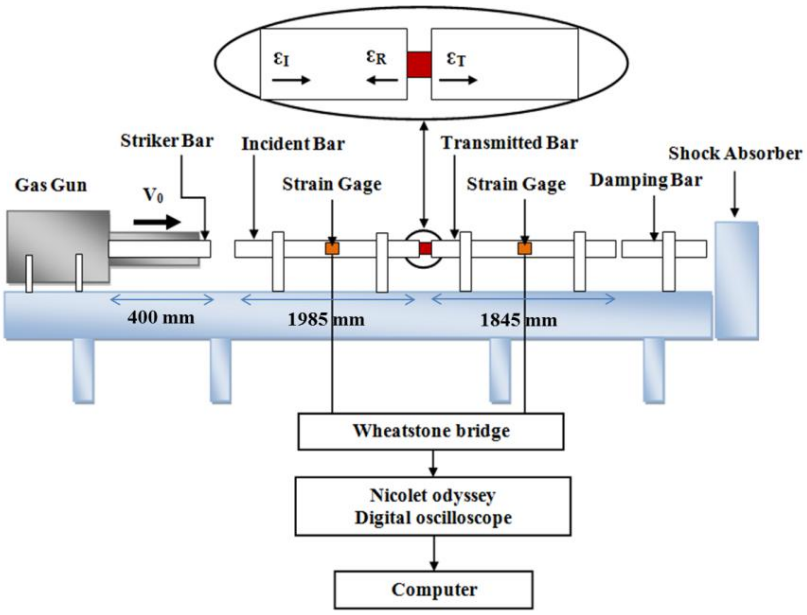
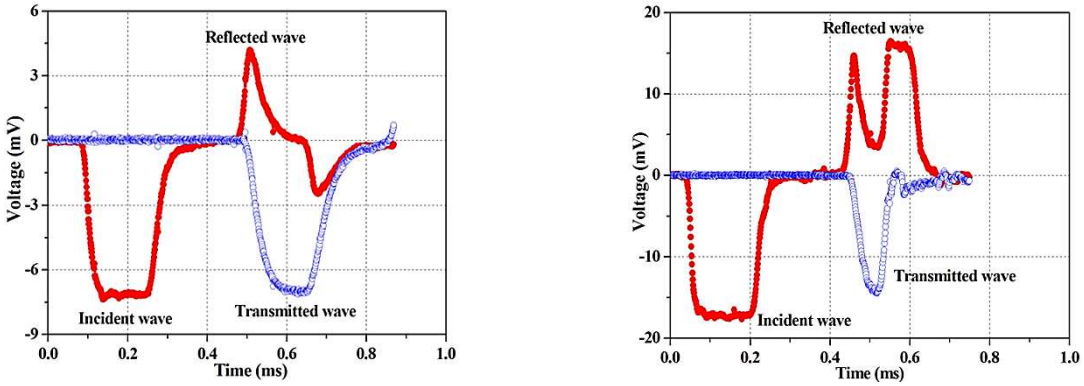


Figure 2: Schematic of the SHPB

The Gas gun as shown in figure 2 is used to launch a striker bar at a specific pressure and hence a specific velocity "V_o". This striker bar impacts the Incident bar thus creating a compression wave which is registered by the Strain gauge in the form of strain "ε_i". The pressure (compression) wave

passes through the specimen, thus applying a high strain rate, dependent on "V_o" and the length of striker bar. A certain part of the applied force "F_i" passes through the specimen and into the Transmitted bar, whose strain is recorded as "ε_t". The transmitted bar is arrested in displacement by the damping bar and a certain part of the compression wave is reflected back through the specimen, recorded as strain "ε_r".

The typical signals registered by the strain gauges at the incident and the transmitted bar are shown as in figure 3. The Damage or Plasticization in the specimen can be seen by the shape of the reflected strain wave.



(a) Test without damage **(b) Test with damage**

Figure 3: Typical no damage and damage signals registered by the strain gauges

In the no damage case the pressure wave is reflected back through the specimen with a fairly elastic response. Whereas in the case of the damage test the reflected wave has two peaks. The first signifying compression at the return then displacement in the fractured or plasticized zone, shown as a loss in transferred strain. The second peak is where the fracture closes and the specimen transfers the reflected force.

As explained the purpose of this apparatus is to apply a given strain rate to the specimens being tested. These basic relations are hence used to determine the applied loads at the given strain rates and to evaluate the effect of strain rate on the mechanical behavior of the composite material.

Loads

Force at incident face $$F_i(t) = A_b E_b[\varepsilon_i(t) + \varepsilon_r(t)]$$ Equation 1

Force at transmitted face $$F_t(t) = A_b E_b \varepsilon_t(t)$$ Equation 2

Velocities

Velocity at incident face $$V_i(t) = -C_o[\varepsilon_i(t) - \varepsilon_r(t)]$$ Equation 3

Velocity at transmitted face $$V_t(t) = C_o\varepsilon_t(t)$$ Equation 4

The parameters of interest at the specimen level are then determined as follows.

Strain Rate

Strain Rate applied at the specimen $$\dot{\varepsilon}(t) = -\frac{2C_o}{L_s}\varepsilon_r(t)$$ Equation 5

Stress

Stress induced in the specimen $$\sigma(t) = \frac{A_b E_b}{A_s}\varepsilon_t(t)$$ Equation 6

Strain

Average strain of the specimen $$\varepsilon(t) = -\frac{2C_o}{L_s}\int_0^t \varepsilon_r(t)dt$$ Equation 7

Where "ε" is the strain, "U" is the voltage applied or measured across a gauge, "F" is the force, "C_o" is the velocity of sound waves, "ν" the Poisson's ratio, "A_b" cross-sectional area of the bars and "E_b" young's modulus of the bar.

b. Specimen Materials

The specimens used are polyester reinforced with fiber glass type composites. The specimens are cut from larger plates manufactured using the vacuum infusion process and cured at room temperature in vacuum. The specimen dimensions are shown in the figure 4.

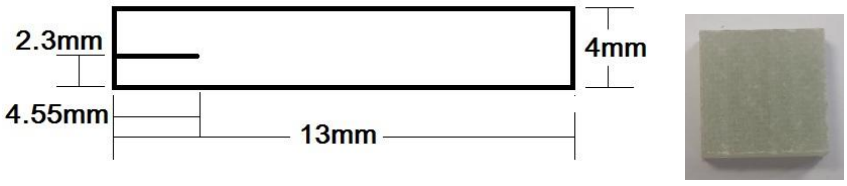


Figure 4: Dimensions of the specimen used

The specimens are 13mm square with a pre-crack of 4.55mm long. The specimens are made up of 7 layers of 45° Biax mat as explained above and have the following properties, as in the Table 1.

Construction	Areal Weight (g/m2)	Tolerance (±%)	Material	Linear Density (tex)
+45°	451	5	E – Glass	600
-45°	451	5	E – Glass	600
Stitching	12	5	PES 76 dtex	
Total Areal weight	912	5	Binder	Warp

Material	Average Modulus (GPa)	Poisson's Ratio	Stress at Failure (MPa)
Uni-directional mat - Fiber direction - Transverse direction	E_L = 48. 11 E_T = 11.21	ν_{LT} = 0.280 ν_{TL} = 0.096	X = 965.50 Y = 33.50
Uni-directional mat in shearing direction	G_{LT} = 4.42	-	48.69

Table 1: Material properties

c. Experimental Procedure

The specimen is placed in the 3 point bending fixture between the two bar ends as shown in the figure 5. The Split Hopkinson Pressure Bar experiment is run under 3 different pressure rates of 0.5, 0.6 and 0.7 bar ranging in a strain rate of 90 – 150 s^{-1}. The pressures are varied to get a variation in the applied strain rates of the specimens.

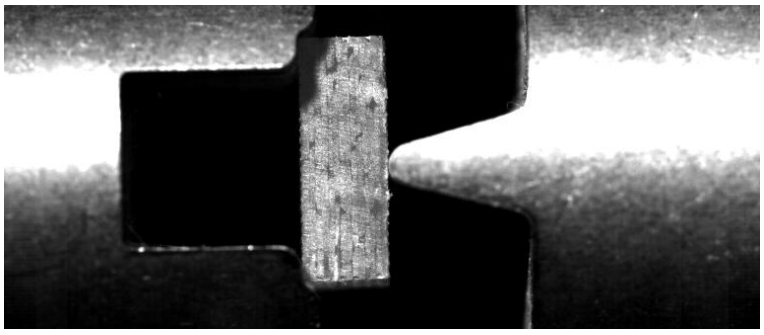
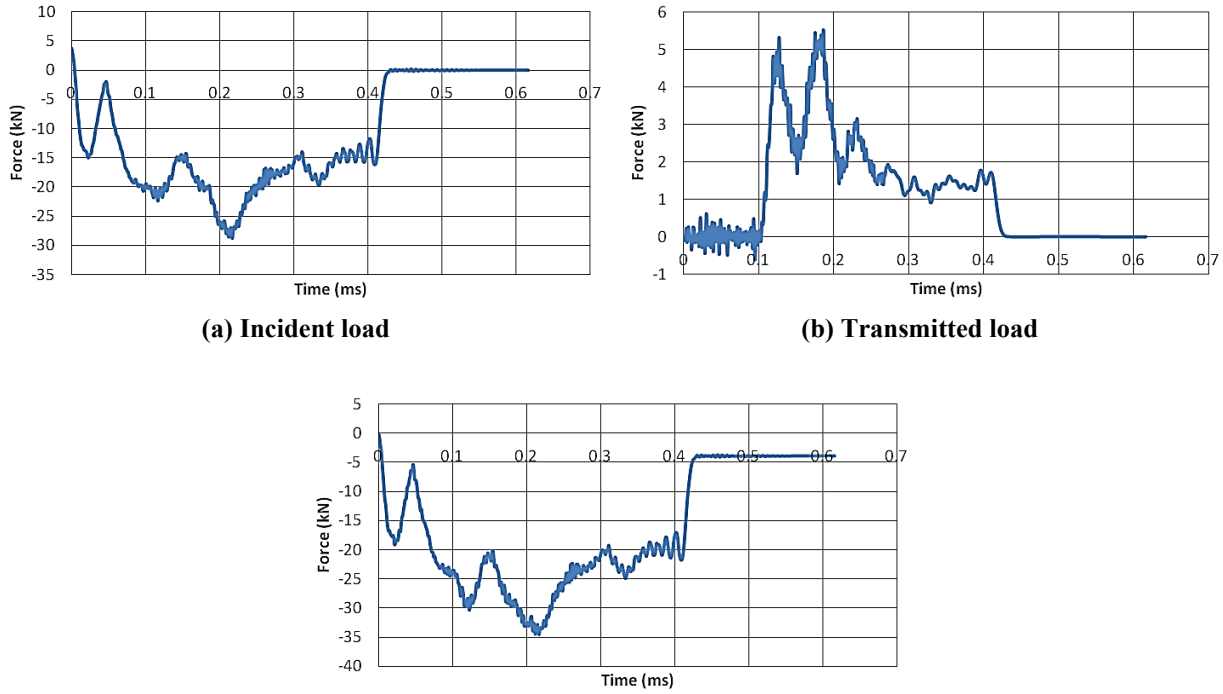


Figure 5: Specimen in position before start of test

The results are later classified according to the applied strain rate at the specimens. The strain rates are calculated in the direction of the application of the force or the transverse strain at the specimen.

B. Dynamic behavior of specimens

The impact force is calculated keeping in line with the Hopkinson bar theory. The typical impact force as shown in the figure 6 is calculated as a difference of the incident and the transmitted forces.



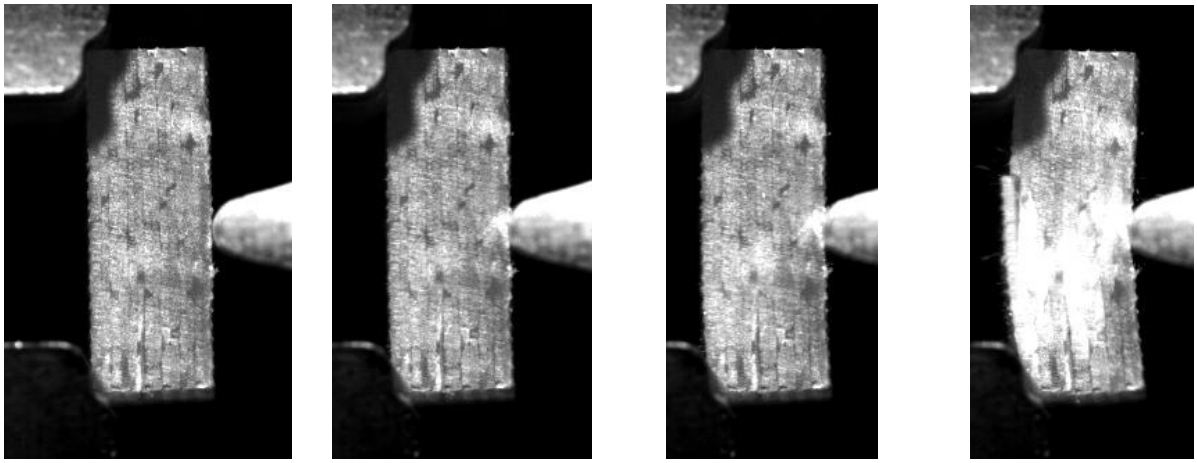
(a) Incident load

(b) Transmitted load

(c) Total applied load

Figure 6: Applied loads

The force curves shown in the figure 6 are the complete force curve for the impact taking place on the specimen. However, on closer inspection it can be seen that the bending phase where the crack propagation takes place is an initial portion of the applied force curve. The figure 7 shows the evolution of the specimen under bending loads as a function of this applied force.



0 – 0.02 (ms) | **0.02 – 0.042 (ms)** | **0.042 – 0.075 (ms)** | **0.075 – 0.1 (ms)**

Figure 7: Evolution of the specimen under applied bending dynamic load

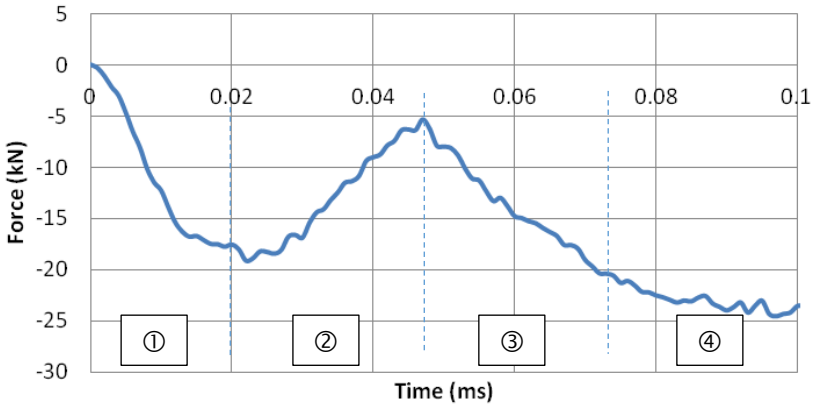


Figure 8: Total applied force on the specimen up to final failure

From the figure 6c the curve in the figure 8 can be partitioned into 4 time-periods:

1: The first up to 0.02 ms represents the first coming in contact of the point on the specimen.

2: The second, 0.02 – 0.042 ms, signifies the setting of the specimen against its supports, or the free rigid body movement till the specimens is hard against the supports.

3: The third, 0.042 – 0.075 ms, the pre-crack propagates and is for our case considered as the time interval where the SERR will be calculated.

4: The last, 0.075 – 0.1 ms, is where the crack reaches the half specimen length and other modes of damage start to appear thus rendering the calculation of SERR impossible using the simple beam theory.

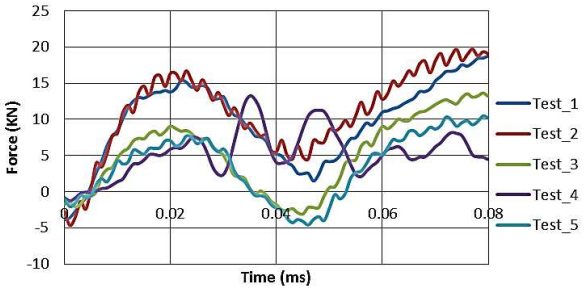
C. Calculation of Mode II SERR

The calculation of the mode II SERR has been done using the Beam Theory approach, although other formulations exist which take into account the variabilities in the crack propagation, however for this study we will use this basic theory to quantify initially just the effect of applied strain rates on the value of Mode II SERR or G_{IIi} [9], [10]. The formulation for the calculation is given as Equation 8.

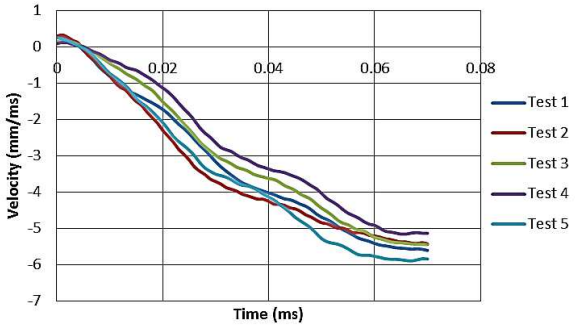
$$G_{11i} = \frac{9a^2Pu}{4L} \qquad \text{Equation 8}$$

Where the "a" is taken as the pre-crack length since the crack propagation is highly abrupt and unstable, "P" is the applied load and "u" is the deflection of the beam specimen calculated by the velocity at the incident bar end, "L" is the length of the specimen given as 13mm.

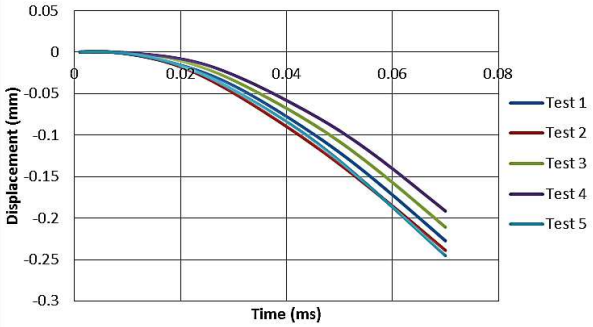
The figure 9 - figure 12 shows the correspondence of the displacement calculated by integrating at each time step the incident bar end velocity and the applied force at the point load.



(a) Applied force

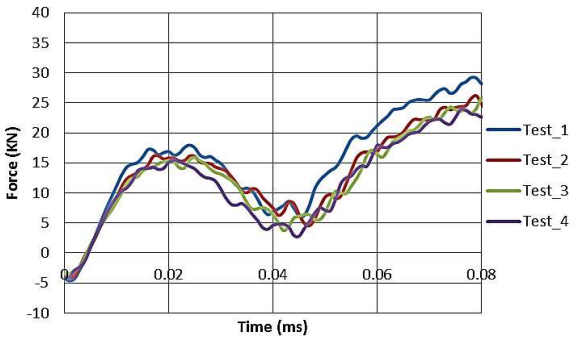


(b) Velocity of the point load

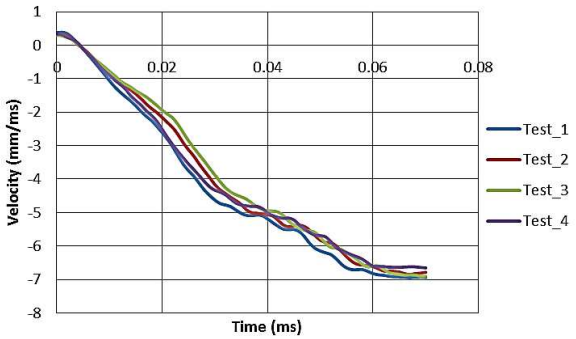


(c) Displacement

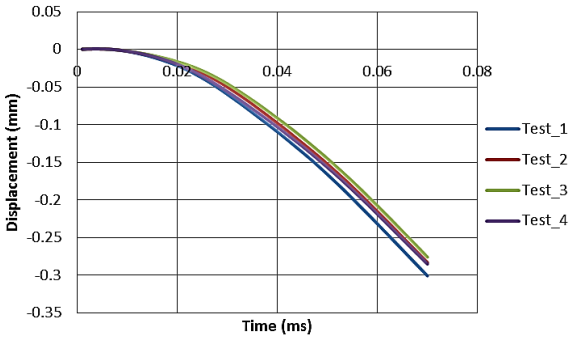
Figure 9: Specimen subjected to 0.5 bar impact pressure



(a) Applied force

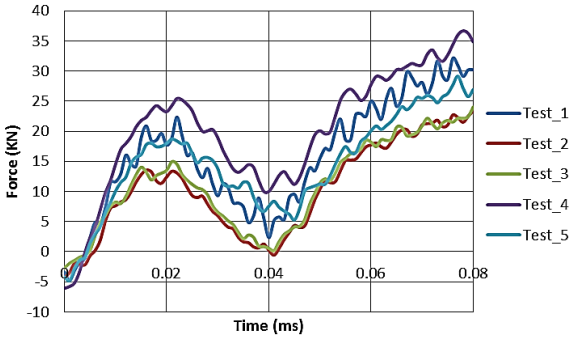


(b) Velocity of the point load

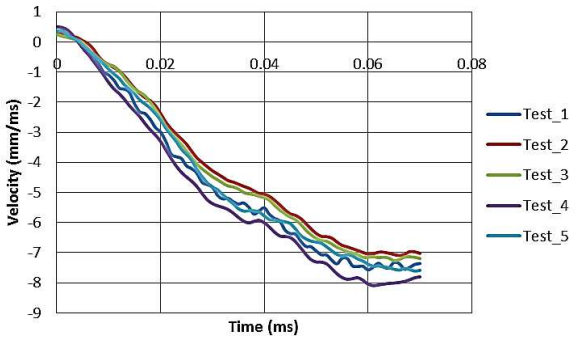


(c) Displacement

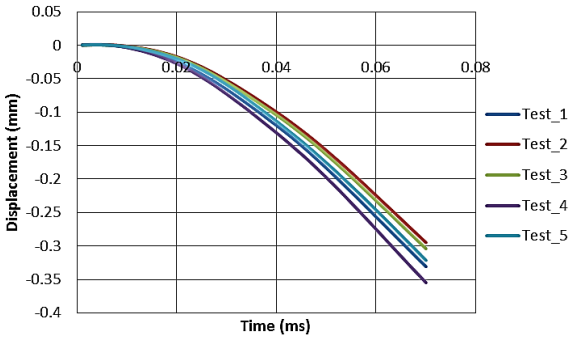
Figure 10: Specimen subjected to 0.6 bar impact pressure



(a) Applied force

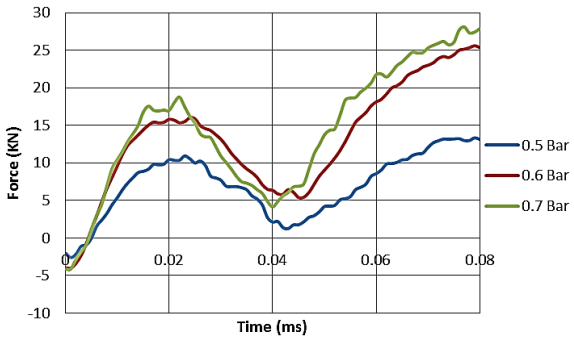


(b) Velocity of the point load

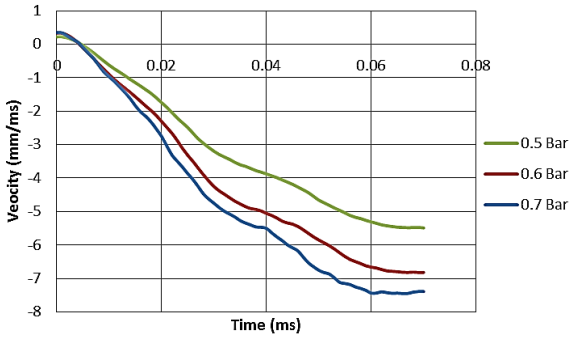


(c) Displacement

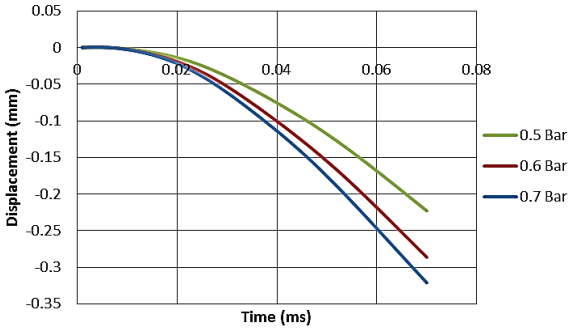
Figure 11: Specimen subjected to 0.7 bar impact pressure



(a) Applied force



(b) Velocity of the point load



(c) Displacement

Figure 12: Specimen subjected to different impact pressure

Considering the applied force and the deflection of the specimen at each of the test pressures and specimens we can calculate the Mode II SERR at the initiation of the crack propagation using the Equation 8. The results can be arranged in terms of applied strain rates, as in Table 2.

0.5 Bar		
G_{IIi} (kJ/m^2)	Strain Rate (s^{-1})	Impact velocity

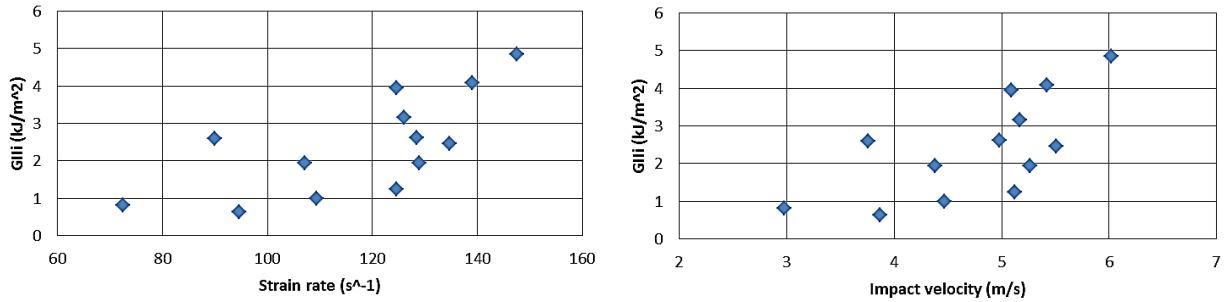
			(m/s)
Test#1	1.94	107.18	4.38
Test#2	2.60	89.93	3.76
Test#3	0.82	72.43	2.98
Test#4	0.99	109.42	4.47
Test#5	0.64	94.56	3.87

	0.6 Bar		
	G_{IIi} (kJ/m^2)	**Strain Rate (s^{-1})**	**Impact velocity (m/s)**
Test#1	3.96	124.64	5.09
Test#2	4.08	139.10	5.42
Test#3	2.63	128.42	4.98
Test#4	3.15	126.07	5.17

	0.7 Bar		
	G_{IIi} (kJ/m^2)	**Strain Rate (s^{-1})**	**Impact velocity (m/s)**
Test#1	2.46	134.64	5.51
Test#2	1.95	128.97	5.26
Test#3	1.25	124.61	5.12
Test#4	7.19	144.94	5.93
Test#5	4.86	147.58	6.02

Table 2: Calculated values of G_{IIi} at different applied strain rates

The values of SERR or G_{IIi} are represented at corresponding strain rates. The tendency of the G_{IIi} is to increase with an increase in the applied strain rate. The figure 13 shows this evolution in the value of G_{IIi} in terms of strain rates and impact velocities.



(a) **(b)**

Figure 13: Evolution of G_{IIi} with (a) applied strain rates, (b) Impact velocity

3. DISCUSSION ON RESULTS

The values of Mode II SERR G_{IIi} have a tendency to increase with the increase of applied strain rates as the impact load is increased as well. However, for this study we have calculated the G_{IIi} at the initiation phase only which can have certain variability due to fiber bridging and as such the initiation process is rather unstable. The static tests have shown a value of G_{IIi} to be in the order of 1.2 kJ/m^2 [8] whereas in the dynamic case it varies from 0.64 to 7.19 kJ/m^2 for the applied strain rates of 70 – 150 s^{-1}.

It should be noted that this range is strongly influenced by a single high-side value (Test #4, 0.7 bar, 144.94 s-1); excluding this point, the remaining tests at this pressure level fall between 1.25 and 4.86 kJ/m^2. Given the small sample size (five tests per pressure level) and the sensitivity of the initiation value of G_{IIi} to fiber bridging and crack-path deviation, this scatter is treated here as an inherent feature of the initiation measurement rather than experimental noise to be discarded. Future work should report mean values with standard deviations over a larger number of repeats at each strain rate to establish the trend with statistical confidence.

The bending tests were done on the same pressure levels to find out the difference of total strain energy released up to total failure. It has been calculated that the un-cracked specimens showed a 16 – 35 % increase in the strain energy liberated as a result of failure under bending loads.

As stated earlier the crack propagation is not stable and is not purely inter-laminar either. Therefore, the energy liberated and calculated as G_{IIi} may be slightly higher than if the crack propagation is purely inter-laminar. As some higher effort is required to diverge the crack in other layers during propagation. Furthermore, the shorter length specimen gives rise to higher shearing stresses as compared to flexural stresses, necessary for the in-plane crack propagation.

4. CONCLUSION

The present study has shown a clear tendency of the crack propagation energy or G_{IIi} in pure shearing to be related to the applied strain rates. However, the values calculated for the Mode II SERR or G_{IIi} need to be refined to isolate purely inter-laminar crack growth. This can likely be achieved by using longer specimen span lengths to reduce the transverse shear stresses in the specimens; shorter specimens were used in this initial study to satisfy the dynamic force-equilibrium requirement of the Hopkinson bar technique. Figure 6 shows that failure occurs at a

near-zero transmitted force, indicating that non-standard or longer specimen geometries could be used to promote stable crack propagation in future tests, provided force equilibrium can still be verified.

5. DATA AVAILABILITY

The data used to support the findings of this study are available from the corresponding author upon request.

6. FUNDING STATEMENT

The Authors of this paper gratefully acknowledge the financial support of the DGA, France (MRIS project).

7. CONFLICTS OF INTEREST

The authors declare that they have no conflicts of interest to report regarding the present study.

8. DECLARATION

The consent is given to publish the manuscript from all authors involved. There is no human or animal related clinical trials involved in the study.

References

[1] F. G. A. Silva, J. J. L. Morais, N. Dourado, J. Xavier, F. A. M. Pereira, and M. De Moura, "Determination of cohesive laws in wood bonded joints under mode II loading using the ENF test," *Int. J. Adhes. Adhes.*, vol. 51, pp. 54–61, 2014.

[2] M. Pankow, A. Salvi, A. M. Waas, C. F. Yen, and S. Ghiorse, "Resistance to delamination of 3D woven textile composites evaluated using End Notch Flexure (ENF) tests: Experimental results," *Compos. Part A Appl. Sci. Manuf.*, vol. 42, no. 10, pp. 1463–1476, 2011.

[3] C. Rubio-González, J. A. Gallardo-González, G. Mesmacque, and U. Sanchez-Santana, "Dynamic fracture toughness of pre-fatigued materials," *Int. J. Fatigue*, vol. 30, no. 6, pp. 1056–1064, 2008.

[4] S. Henschel and L. Krüger, "Dynamic crack initiation measurements in a four-point split Hopkinson bending device," *Eng. Fract. Mech.*, vol. 133, pp. 62–75, 2015.

[5] S. N. Nwosu, D. Hui, and P. K. Dutta, "Dynamic mode II delamination fracture of unidirectional graphite/epoxy composites," *Compos. Part B Eng.*, vol. 34, no. 3, pp. 303–316, 2003.

[6] D. Li, H. Chen, D. Ge, N. Jiang, and L. Jiang, "Split Hopkinson pressure bar testing of 3D multi-axial warp knitted carbon/epoxy composites," *Compos. Part B Eng.*, vol. 79, pp. 692–705, 2015.

[7] M. F. Omar, H. M. Akil, Z. A. Ahmad, A. A. M. Mazuki, and T. Yokoyama, "Dynamic properties of pultruded natural fibre reinforced composites using Split Hopkinson Pressure Bar technique," *Mater.*

\& *Des.*, vol. 31, no. 9, pp. 4209–4218, 2010.

[8] O. R. Shah and M. Tarfaoui, “Effect of adhesive thickness on the Mode I and II strain energy release rates. Comparative study between different approaches for the calculation of Mode I \& II SERR’s,” *Compos. Part B Eng.*, vol. 96, pp. 354–363, 2016.

[9] A. B. De Morais, “Novel cohesive beam model for the End-Notched Flexure (ENF) specimen,” *Eng. Fract. Mech.*, vol. 78, no. 17, pp. 3017–3029, 2011.

[10] A. Shojaei, G. Li, P. J. Tan, and J. Fish, “Dynamic delamination in laminated fiber reinforced composites: A continuum damage mechanics approach,” *Int. J. Solids Struct.*, vol. 71, pp. 262–276, 2015.

[11] H. Zabala, L. Aretxabaleta, G. Castillo, and J. Aurrekoetxea, "Dynamic 4ENF test for a strain rate dependent mode II interlaminar fracture toughness characterization of unidirectional carbon fibre epoxy composites," Polym. Test., vol. 55, pp. 212–218, 2016.

[12] M. Yasaee, G. Mohamed, A. Pellegrino, N. Petrinic, and S. R. Hallett, "Strain rate dependence of mode II delamination resistance in through thickness reinforced laminated composites," *Int. J. Impact Eng.*, vol. 107, pp. 1–11, 2017.

[13] S. P. Shamchi, M. F. S. F. de Moura, Z. Zhao, X. Yi, and P. M. G. P. Moreira, "Dynamic mode II interlaminar fracture toughness of electrically modified carbon/epoxy composites," *Int. J. Impact Eng.*, vol. 159, art. no. 104030, 2022.

[14] J. J. M. Machado, E. A. S. Marques, R. D. S. G. Campilho, and L. F. M. da Silva, "Mode II fracture toughness of CFRP as a function of temperature and strain rate," *Compos. Part B Eng.*, vol. 114, pp. 311–318, 2017.

[15] K. O. Low, M. Johar, H. A. Israr, K. W. Gan, S. S. Rahimian Koloor, M. Petrů, and K. J. Wong, "Displacement rate effects on the mode II shear delamination behavior of carbon fiber/epoxy composites," *Polymers*, vol. 13, no. 11, art. 1881, 2021.

[16] M. May et al., "High-rate mode II fracture toughness testing of polymer matrix composites – A review," *Compos. Part A Appl. Sci. Manuf.*, vol. 137, art. 106019, 2020.

[17] A. J. Smiley and R. B. Pipes, "Rate effects on mode I interlaminar fracture toughness in composite materials," *J. Compos. Mater.*, vol. 21, no. 7, pp. 670–687, 1987.

[18] A. A. Aliyu and I. M. Daniel, "Effects of strain rate on delamination fracture toughness of graphite/epoxy," in *Delamination and Debonding of Materials*, ASTM STP 876, W. S. Johnson, Ed. Philadelphia, PA: ASTM, 1985, pp. 336–348.

[19] I. M. Daniel, I. Shareef, and A. A. Aliyu, "Rate effects on delamination fracture toughness of a toughened graphite/epoxy," in *Toughened Composites*, ASTM STP 937, N. J. Johnston, Ed. Philadelphia, PA: ASTM, 1987.

[20] A. B. de Morais, J. F. Silva, and A. T. Marques, "Mode II interlaminar fracture of filament wound angle-ply specimens," *Appl. Compos. Mater.*, vol. 9, pp. 117–129, 2002.

[21] W. S. Ekeoseye, K. Kolasangiani, D. C. D. Oguamanam, and H. Bougherara, "Mode II interlaminar fracture toughness of flax/glass/epoxy hybrid composite materials: An experimental and numerical study," *J. Nat. Fibers*, vol. 19, no. 11, pp. 4286–4300, 2022.

[22] L. A. Carlsson, J. W. Gillespie Jr., and B. R. Trethewey, "Mode II interlaminar fracture of graphite/epoxy and graphite/PEEK," *J. Reinf. Plast. Compos.*, vol. 5, p. 170, 1986.

[23] A. J. Russell and K. N. Street, "Moisture and temperature effects on the mixed-mode delamination fracture of unidirectional graphite/epoxy," in *Delamination and Debonding of Materials*, ASTM STP 876, W. S. Johnson, Ed. Philadelphia, PA: ASTM, 1985, p. 349.

[24] K. Friedrich, R. Walter, L. A. Carlsson, A. J. Smiley, and J. W. Gillespie Jr., "Mechanisms for rate effects on interlaminar fracture toughness of carbon/epoxy and carbon/PEEK composites," *J. Mater. Sci.*, vol. 24, pp. 3387–3398, 1989.

[25] I. M. Daniel, W. G. Hamilton, and R. H. Labedz, "Strain rate characterization of unidirectional graphite/epoxy composite," in *Composite Materials: Testing and Design (Sixth Conf.)*, ASTM STP 787, I. M. Daniel, Ed. Philadelphia, PA: ASTM, 1982, pp. 393–413.

[26] F. Ozdil, L. A. Carlsson, and P. Davies, "Beam analysis of angle-ply laminate end-notched flexure specimens," *Compos. Sci. Technol.*, vol. 58, pp. 1929–1938, 1998.

[27] B. D. Davidson, R. Krüger, and M. König, "Three-dimensional analysis and resulting design recommendations for unidirectional and multidirectional end-notched flexure tests," *J. Compos. Mater.*, vol. 29, pp. 2108–2133, 1995.

[28] G. C. Jacob, J. M. Starbuck, J. F. Fellers, S. Simunovic, and R. G. Boeman, "Fracture toughness in random-chopped fiber-reinforced composites and their strain rate dependence," *J. Appl. Polym. Sci.*, vol. 100, no. 1, pp. 695–701, 2006.

[29] R. Gerlach, C. R. Siviour, J. Wiegand, and N. Petrinic, "The strain rate dependent material behavior of S-GFRP extracted from GLARE," *Mech. Adv. Mater. Struct.*, vol. 20, no. 7, pp. 505–514, 2013.

[30] H. Kolsky, "An investigation of the mechanical properties of materials at very high rates of loading," *Proc. Phys. Soc. B*, vol. 62, no. 11, pp. 676–700, 1949.

[31] B. Hopkinson, "A method of measuring the pressure produced in the detonation of high explosives or by the impact of bullets," *Philos. Trans. R. Soc. A*, vol. 213, pp. 437–456, 1914.

[32] L. Rubio, J. Fernández-Sáez, and C. Navarro, "Determination of dynamic fracture-initiation toughness using three-point bending tests in a modified Hopkinson pressure bar," *Exp. Mech.*, vol. 43, no. 4, pp. 379–386, 2003.

[33] R. Chen, K. Xia, F. Dai, F. Lu, and S. N. Luo, "Determination of dynamic fracture parameters using a semi-circular bend technique in split Hopkinson pressure bar testing," *Eng. Fract. Mech.*, vol. 76, pp. 1268–1276, 2009.

[34] A. S. D. Wang, M. Slomiana, and R. B. Bucinell, "Delamination crack growth in composite laminates," in *Delamination and Debonding of Materials*, ASTM STP 876, W. S. Johnson, Ed. Philadelphia, PA: ASTM, 1985, pp. 135–167.

[35] S. Liu, Z. Kutlu, and F. K. Chang, "Matrix cracking and delamination in laminated composite beams subjected to a transverse concentrated line load," *J. Compos. Mater.*, vol. 27, no. 5, pp. 436–470, 1993.

[36] M. D. Gilchrist and N. Svensson, "A fractographic analysis of delamination within multidirectional carbon/epoxy laminates," *Compos. Sci. Technol.*, vol. 55, pp. 195–207, 1995.

[37] D. J. Boll, D. L. Hunston, B. Fuller, and P. J. Phillips, "Fractographic analysis of interlaminar fracture," in *Toughened Composites*, ASTM STP 937, N. J. Johnston, Ed. Philadelphia, PA: ASTM, 1987, pp. 131–149.

[38] J. A. Nairn, "Energy release rate analysis for adhesive and laminate double cantilever beam specimens emphasizing the effect of residual stresses," *Int. J. Adhes. Adhes.*, vol. 20, pp. 59–70, 2000.

[39] J. Wiegand, A. Hornig, R. Gerlach, C. Neale, N. Petrinic, and W. Hufenbach, "An experimental method for dynamic delamination analysis of composite materials by impact bending," *Mech. Adv. Mater. Struct.*, 2016.

[40] B. D. Davidson, R. Krüger, and M. König, "Effect of stacking sequence on energy release rate distributions in multidirectional DCB and ENF specimens," *Eng. Fract. Mech.*, vol. 55, no. 4, pp. 557–569, 1996.